Annals of Biomedical Engineering, Vol. 31, pp. 972–980, 2003
Printed in the USA.

0090-6964/2003/31(8)/972/9/$20.00

Three-Dimensional Computational Fluid Dynamics Modeling of Alterations in Coronary Wall Shear Stress Produced by Stent Implantation

JOHN F. LADISA, JR.,[1,4] ISMAIL GULER,[5] LARS E. OLSON,[4] DOUGLAS A. HETTRICK,[1,4] JUDY R. KERSTEN,[1,3] DAVID C. WARLTIER,[1,2,3,4] AND PAUL S. PAGEL[1,3,4]

[1]Department of Anesthesiology, [2]Department of Medicine (Division of Cardiovascular Diseases), [3]Department of Pharmacology and Toxicology, the Medical College of Wisconsin and the Clement J. Zablocki Veterans Affairs Medical Center, Milwaukee, WI; [4]Department of Biomedical Engineering, Marquette University, Milwaukee, WI; and [5]Boston Scientific—Scimed, Maple Grove, MN

(Received 8 April 2002; accepted 18 April 2003)

Abstract—Rates of coronary restenosis after stent implantation vary with stent design. Recent evidence suggests that alterations in wall shear stress associated with different stent types and changes in local vessel geometry after implantation may account for this disparity. We tested the hypothesis that wall shear stress is altered in a three-dimensional computational fluid dynamics (CFD) model after coronary implantation of a 16 mm slotted-tube stent during simulations of resting blood flow and maximal vasodilation. Canine left anterior descending coronary artery blood flow velocity and interior diameter were used to construct CFD models and evaluate wall shear stress proximal and distal to and within the stented region. Channeling of adjacent blood layers due to stent geometry had a profound affect on wall shear stress. Stagnation zones were localized around stent struts. Minimum wall shear stress decreased by 77% in stented compared to unstented vessels. Regions of low wall shear stress were extended at the stent outlet and localized to regions where adjacent axial strut spacing was minimized and the circumferential distance between struts was greatest within the stent. The present results depict alterations in wall shear stress caused by a slotted-tube stent and support the hypothesis that stent geometry may be a risk factor for restenosis by affecting local wall shear stress distributions. © *2003 Biomedical Engineering Society.*
[DOI: 10.1114/1.1588654]

Keywords—Shear stress, Coronary hemodynamics, Slotted-tube endovascular stents, Vascular prosthesis, Coronary artery disease, Numerical modeling, Intimal hyperplasia, Restenosis.

INTRODUCTION

Stents are commonly used to restore blood flow in patients with severe coronary artery disease, but restenosis remains a persistent problem in a substantial number of patients treated with this modality.[7,8,37] The incidence and severity of restenosis appears to vary with stent type.[10,13,35,39,42] These data suggest that stent geometry and its subsequent effects on localized fluid dynamics may be risk factors for restenosis. Previous computational fluid dynamics (CFD) modeling studies have used vascular geometries that approximate the stented region of the vessel and focus primarily on the most prominent areas of restenosis, that is, the inlet and outlet of the stent.[3,40,41] These studies provide evidence that localized vessel geometry is a major factor influencing wall shear stress distributions and support the well-established observation that areas of maximal intimal thickening correlate with regions of low and oscillatory wall shear stress.[15,17,20,21,30] Localized alterations in wall shear rate within the stented portion of a vessel have been studied using a two-dimensional (2D) CFD model,[3] but three-dimensional (3D) computational investigations that use a realistic stent geometry to consider the interaction between intricacies in stent design and their consequent actions on distributions of wall shear stress have yet to be conducted. We developed a series of three-dimensional CFD models to test the hypothesis that distributions of wall shear stress during resting coronary blood flow and maximal coronary vasodilation are altered by the presence of a slotted-tube stent.

METHODS

All experimental procedures and protocols used in this investigation were reviewed and approved by the Animal Care and Use Committee of the Medical College of Wisconsin and Marquette University. All conformed to the *Guide for the Care and Use of Laboratory Animals* of the National Institutes of Health (7th ed. Washington, DC: Nat. Acad. Press, 1996).

Experimental Preparation and Protocol

Computational simulations were based on *in vivo* measurements of canine left anterior descending (LAD)

Address correspondence to Paul S. Pagel, MD, PhD, Medical College of Wisconsin, MEB-M4280, 8701 Watertown Plank Road, Milwaukee, WI 53226. Electronic mail: pspagel@mcw.edu

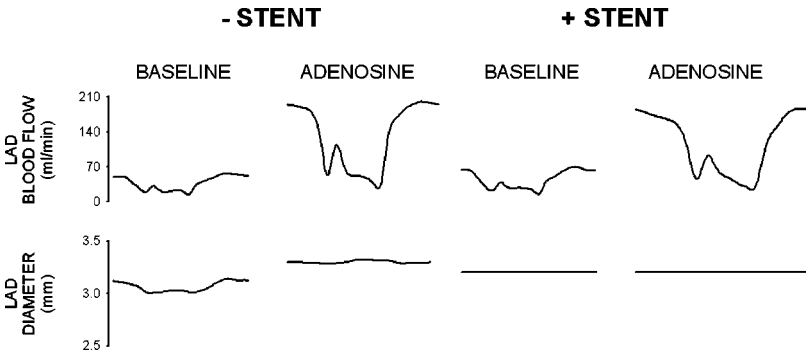

FIGURE 1. Ensemble averaged left anterior descending coronary artery (LAD) blood flow and external diameter waveforms obtained under base line conditions and during the administration of adenosine (1.0 mg/min) in the absence (−stent) and presence (+stent) of an intracoronary stent.

coronary artery diameter and blood flow velocity before and after placement of a slotted-tube stent (NIR, Medinol Ltd., Jerusalem, Israel) in the absence or presence of a 20 min infusion of the coronary vasodilator adenosine (1.0 mg/ml).[18] External LAD diameter was determined by placing a 2.5–3.0 mm ultrasonic segment length transducer (Iowa Doppler Products, Iowa City, IA) around the stented region of the coronary artery. The LAD coronary artery was assumed to have concentric radial properties, negligible taper, and exposure to the same diameter waveform along the axial length of the vascular region of interest.[26] Internal LAD radius (r_i) was determined using the equation: $r_i = (r_o^2 - V/L\pi)^{1/2}$, where r_o is the external LAD radius, L is the length of the vessel in the region of interest *in situ*, and V is the ratio of the excised vessel weight to density (assumed to be 1.06 g/ml).[24] Blood flow was recorded by using a transit-time flow probe (Transonic Systems, Ithaca, NY) positioned around the proximal LAD coronary artery. Additionally, left ventricular pressure (LVP) was simultaneously recorded for use in signal processing. A representative time series for LAD blood flow and diameter were created using a Matlab program that aligned each variable according to peak LVP, segmented each digitized variable waveform into individual cardiac cycles, and ensemble averaged the segments (Fig. 1).

Construction of Computational Arteries

Computational arteries were created by entering *in vivo* internal diameter values corresponding to each intervention (Table 1) and stent properties including the number of struts, strut thickness, and stent length into a geometric construction and mesh generation algorithm custom designed using Matlab. Computational geometries for each intervention were composed of structured hexahedral control volumes arranged in a four-domain butterfly design (Fig. 2) that exploits symmetric stent and vessel properties to create half of the computational vessel. The stent geometry created for this investigation was based on the Palmaz–Schatz slotted-tube design in order for comparison with results from previous studies.[4,11,23,31] The axial size of hexahedral elements proximal, distal, and within the stented region was one fourth that of other portions of stented or unstented vessels. All computational stent geometries contained four circumferential and axial repeating stent struts and were 16 mm in length. Computational stent struts were approximately 0.35 mm wide, fully opposed to the vessel wall, and protruded 0.1 mm into the flow domain.[13]

Computational Model Simulations

Unstented and stented computational geometries were imported into a commercially available software package (CFD-ACE, Computational Fluid Dynamics Research Corporation, Huntsville, AL) for analysis of shear stress distributions along the vessel wall. This software uses a finite volume approach to solve equations satisfying conservation of mass and momentum at the center of each hexahedral control volume. Simulations were conducted by imposing minimum and maximum coronary blood flow velocities ($w_{\min}$ and $w_{\max}$, respectively; Fig. 3) from each *in vivo* intervention as steady-state parabolic

TABLE 1. Simulation properties.

	Base line		Adenosine		Stent		Stent + adenosine	
	Minimum	Maximum	Minimum	Maximum	Minimum	Maximum	Minimum	Maximum
Velocity (cm/s)	3.30	15.8	8.30	58.2	5.30	22.5	3.30	45.9
Diameter (mm)	2.51	2.60	2.59	2.63	2.74	2.74	2.74	2.74

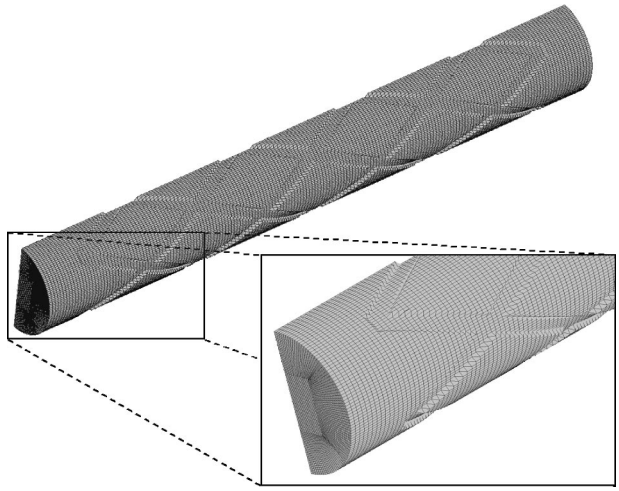

FIGURE 2. Computational geometry representing a slotted-tube stent. The computational mesh represents the blood flow domain through the stented region of the vessel.

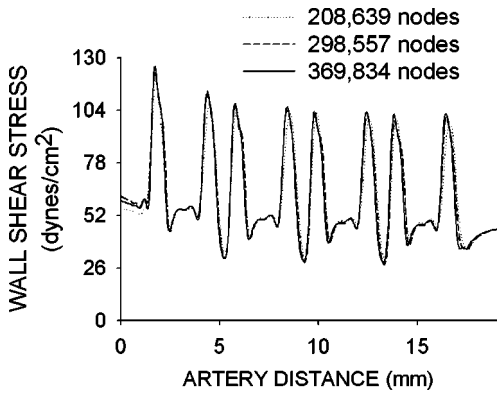

FIGURE 4. Evaluation of mesh independence for axisymmetryic stented computational vessels. Axial distributions of wall shear stress vs. artery length for vessels containing 208,639; 298,557; and 369,834 nodes that were subjected to the same inlet velocity. Simulations were performed using the inlet velocity obtained during maximum coronary artery vasodilation with adenosine.

profiles calculated from the flow rate and the cross-sectional area of the vessel. Pressure at the vessel outlet was set to zero, which enabled the flow solver to calculate the pressure gradient within the flow domain. All computational simulations were conducted assuming a Newtonian, incompressible fluid with a density of 1060 kg/m^3 and viscosity of 3.7 cP. Simulations were performed on Silicon Graphics O_2 5k computers with 1 Gbyte of RAM and convergence was, typically, obtained after 24–72 h. Simulation results were examined as color map distributions of wall shear stress.

Determination of Wall Shear Stress

Wall shear stress was determined as the product of viscosity and wall shear rate ($\dot{\gamma}$). The CFD-ACE flow solver calculates shear rate from the second invariant of the strain-rate tensor. The shear rate is, therefore, calculated in Cartesian coordinates as

$$\dot{\gamma}=[2\{(\partial u/\partial x)^2+(\partial v/\partial y)^2+(\partial w/\partial z)^2\}+(\partial u/\partial y+\partial v/\partial x)^2+(\partial u/\partial z+\partial w/\partial x)^2+(\partial v/\partial z+\partial w/\partial y)^2]^{1/2},$$

where u, v, and w are the x, y, and z components of the velocity vector, respectively. In a simple shear flow, $\dot{\gamma}$ reduces to the velocity gradient.

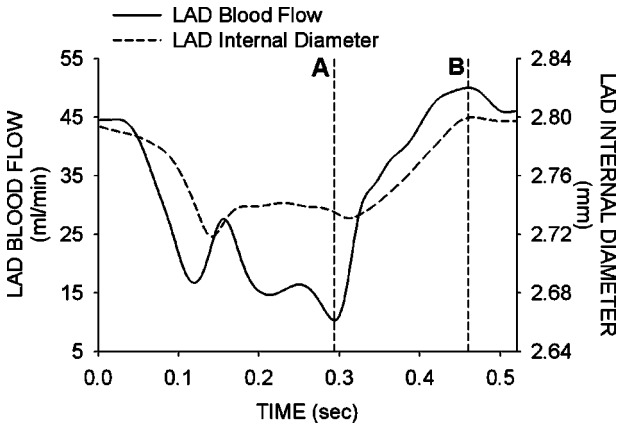

FIGURE 3. Ensemble averaged canine LAD blood flow and interior diameter waveforms during base line conditions. Steady-state minimum (A) and maximum (B) blood flow values imposed as inlets to model simulations are indicated by the dashed lines intersecting each waveform.

RESULTS

Refinement of the Computational Mesh

The number of circumferential nodes along the perimeter and the spacing of axial nodes along the length of unstented vessels were varied systematically until distributions of wall shear stress closely approximated the theoretical value determined as $\tau=4\mu Q/\pi r^3$, where Q is the blood flow rate, r is the radius of the vessel, and μ is the viscosity. Mesh independence was investigated for stented vessels by comparing distributions of wall shear stress in vessels with 208,639; 298,557; and 369,834 nodes, which were subjected to the peak inlet velocity obtained during maximum coronary artery vasodilation with adenosine (Fig. 4). Simulation results were assumed to be independent of the computational mesh when the disparity between meshes of varying densities was less than 6%.[22]

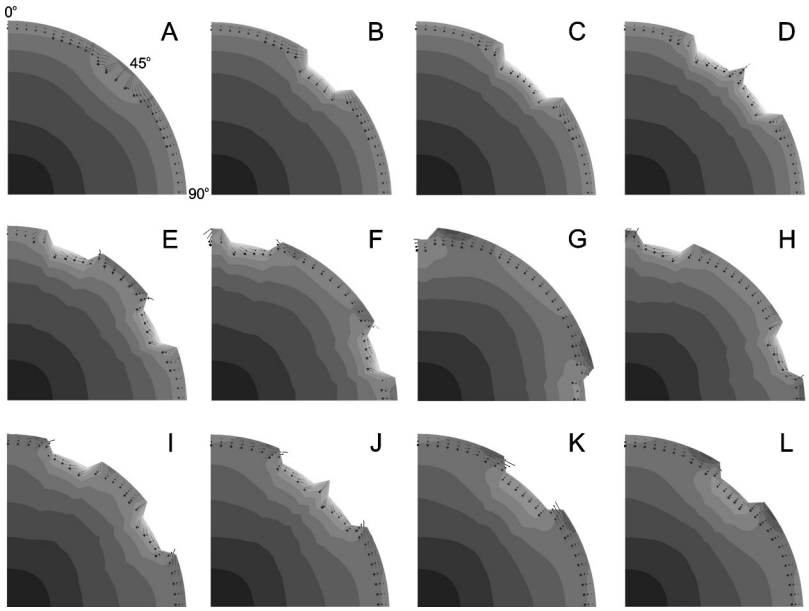

FIGURE 5. Directional alterations in near-wall velocity in response to the presence of a slotted-tube stent. The trajectory of adjacent blood layers is denoted by arrows superimposed on cross-sectional distributions of wall shear stress immediately proximal to the stent (panel A) and proceeding through the first 4 mm of the computational vessel (panels B–L).

Velocity Vector Alterations in Stented Vessels

Blood flow through unstented computational vessels was comprised only of the w component of the velocity vector. In contrast, the presence of the stent caused profound out-of-plane motion of the u and v components of the velocity vector. The behavior of near-wall velocity as blood enters and proceeds through the stented region is demonstrated in Fig. 5. Blood encountering the proximal edge of the stent is forced toward the center of the vessel immediately prior to entering the stent [Fig. 5(A)]. The geometry of the stent causes channeling of blood layers adjacent to the stent [Fig. 5(B)] while those directly over the strut are forced toward the center of the vessel [Fig. 5(C)]. Adjacent blood layers nearest 45° are then allowed to separate after passing over the proximal stent edge [Fig. 5(D)]. As blood layers nearest 0° and 90° continue to converge, those closest to 45° begin to diverge as they enter the portion of the stent resembling a diverging nozzle [Figs. 5(E) and 5(F)]. Converging and diverging blood layers then meet at the first point of increased cross-sectional area within the stented portion of the vessel [Fig. 5(G)]. Blood layers nearest 0° and 90° then begin diverging while those nearest 45° are channeled together [Figs. 5(H), 5(I), and 5(J)]. Converging and diverging blood layers once again meet while exiting the first axial stent diamond [Figs. 5(K) and 5(L)], and this pattern is repeated along the length of the stented vessel.

Distributions of Wall Shear Stress

Wall shear stress for unstented vessels corresponding to w_{min} boundary conditions were constant at 3.8 and 9.5 dyn/cm^2 for base line and adenosine simulations, respectively. Wall shear stress for resting and adenosine simulations during w_{max} boundary conditions were 18 and 65 dyn/cm^2, respectively. A representative wall shear stress color map within the stented region of the computational vessel is shown in Fig. 6. Distributions of wall shear stress along several axial lines are also plotted as a function of distance through the stented region of the computational vessel (Fig. 7).

Stent geometry had a dramatic effect on distributions of wall shear stress. The highest wall shear stress values occurred over the surface of stent struts. Wall shear stress values decreased modestly with each subsequent strut. Regions of low wall shear stress were observed before and after each stent strut. A bimodal distribution of elevated wall shear stress occurred between struts and progressively decreased in magnitude downstream. Regions of high wall shear stress immediately proximal to the first strut dissipate from the center of the computational domain to the junction of adjacent domains, concomitant with the elevation of shear stress values over the stent struts that protrude into the flow domain. Areas of low wall shear stress were noticed at transitions between the vessel and stent and were most pronounced where the strut orientation was orthogonal to the direction of blood flow. In addition, an extended region of low wall shear stress was noted at the outlet of the stent.

Maximum wall shear stress (τ_{max}) within the stented region was localized along the axial line where angled stent struts meet in the center of the flow domain for all input velocity simulations, with the exception of the high wall shear stress observed directly over the struts. In contrast, minimum wall shear stress (τ_{min}) within the local vicinity of the stent occurred along the axial line

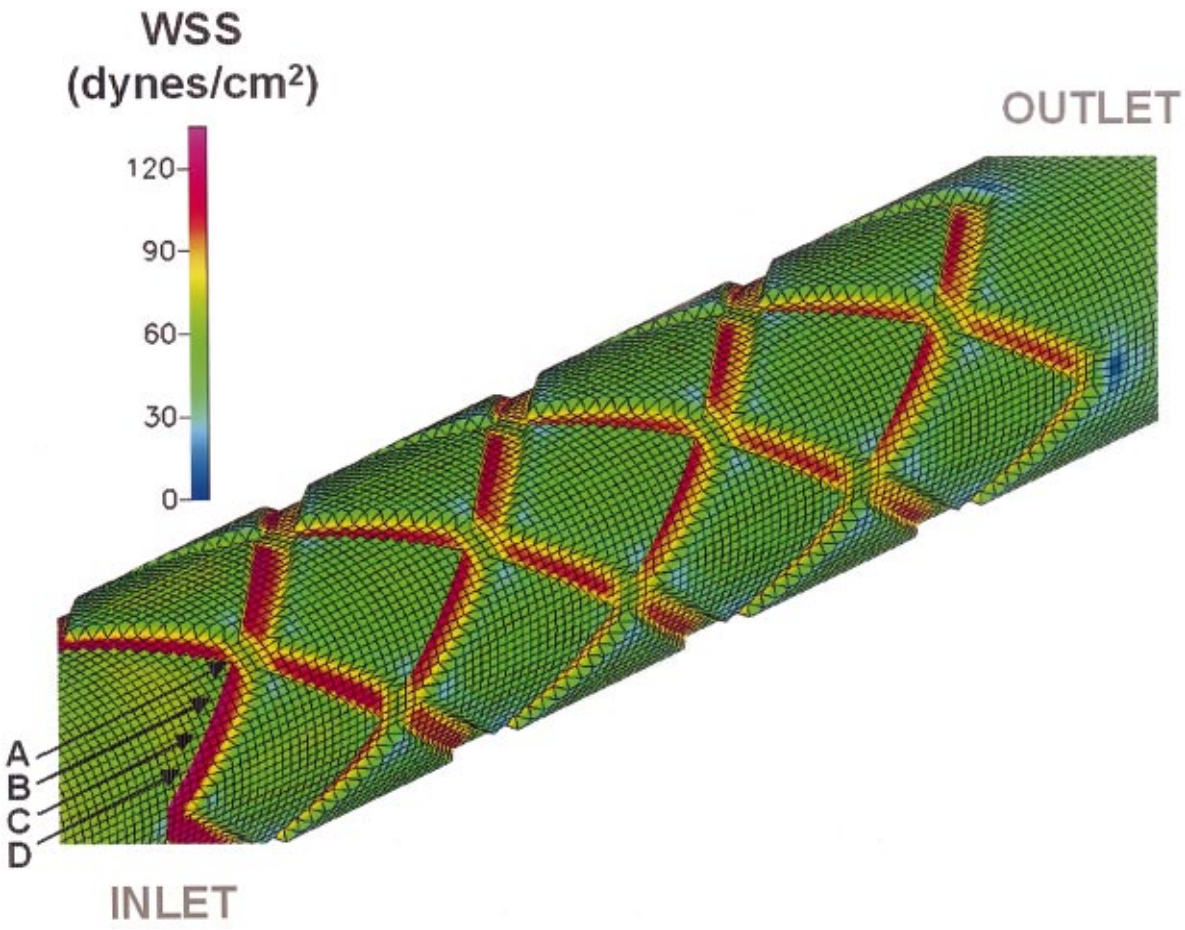

FIGURE 6. Wall shear stress contour plot illustrating the assignment of axial lines within the stented region of the computational artery. Axial line numbering begins in the center of the first converging nozzle (A) and proceeds toward the junction of adjacent perimeter domains (D).

denoted by axial line D in Fig. 8, independent of input velocity.

Minimum wall shear stress at the outlet of the stent was reduced for w_{min} and w_{max} during conditions of resting blood flow as compared to unstented interventions (18% and 51%, respectively). This change was more pronounced for inputs corresponding to elevated blood flow (77% for both). Similarly, τ_{min} decreased by 53% and 74% for minimum and maximum boundary conditions during elevated blood flow proximal to the stent and by 66% and 82% within the stent. Resting boundary conditions for w_{min} and w_{max} simulations in stented computational vessels caused a 3% increase and a 12% decrease in proximal τ_{min}, respectively, compared to unstented vessels. Resting boundary conditions for w_{min} and w_{max} caused a 30% increase and 13% decrease in τ_{min} within the stented region, respectively, compared to unstented computational vessels.

DISCUSSION

Endovascular stents improve resting coronary blood flow and increase flow reserve in the presence of stenoses. However, the impact of stent geometry on local fluid dynamics and wall shear stress within the stented region remains largely unknown. Several studies have examined the time course and physiological consequences of restenosis after stent placement,[6,28,29] but the influence of alterations in local wall shear stress distributions after implantation on the probability of restenosis has not been investigated thoroughly. The vascular endothelium elicits compensatory mechanisms to maintain normal wall shear stress within 15–20 dyn/cm^2.[16] Nonetheless, it is well documented that regions of high shear stress (greater than 12 dyn/cm^2) protect against intimal hyperplasia while a strong correlation between regions of maximal intimal thickening and areas of low (less than 4 dyn/cm^2) and oscillatory wall shear stress has been previously described.[17,20,21] Vascular responses resulting from stent implantation may persist for up to three months after deployment.[37] Recent evidence suggests that local shear stress distributions imposed on the vessel after vascular injury may influence the response of surrounding smooth muscle cells, an important component of intimal hyperplasia.[6,19] Intimal hyperplasia has been

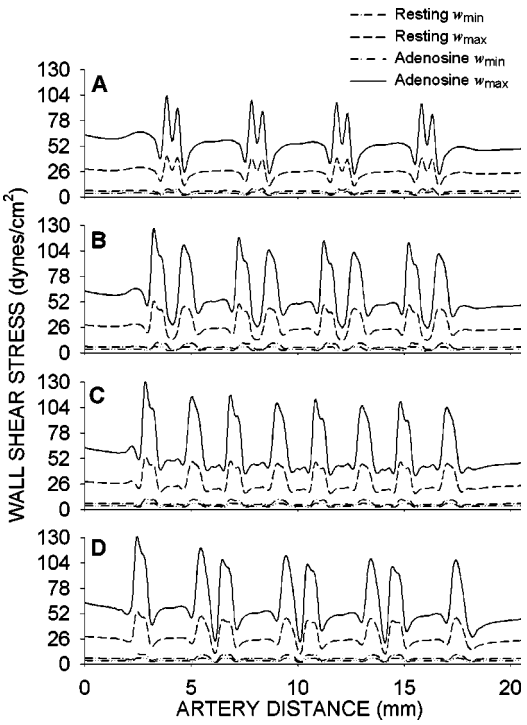

FIGURE 7. Shear stress plotted vs. axial distance along axial lines A, B, C, and D for the minimum and maximum resting and coronary vasodilation input velocity simulations. Wall shear stress distributions were symmetric about the center node of each domain.

noted at the proximal and distal ends of implanted stents,[11] a finding that suggests that altered distributions of wall shear stress may contribute to restenosis in these areas. Collectively, these data support the contention that stent geometry and the effects of stents on the distribution of wall shear stress may represent risk factors for intimal hyperplasia and may also partially explain the disparity observed between the rates of restenosis among different stent designs.

The three-dimensional results of the present investigation indicate that the presence of a computational slotted-tube stent causes profound alterations in near-wall velocity and wall shear stress patterns when compared to an unstented vessel. The major findings of the investigation are summarized in Fig. 8 and illustrate the importance of stent geometry in influencing distributions of wall shear stress. Convergence and divergence of adjacent blood layers occurs to satisfy continuity as the vessel area changes from the presence of the stent along each axial disk that collectively constitute the computational vessel (Fig. 5). Low wall shear stress was observed near the center of each axial diamond where the cross-sectional area of the vessel increases. These portions of the vessel may represent locations where stagnation of blood could occur, rendering them more susceptible to thrombus formation, platelet accumulation, and smooth muscle cell proliferation.[3,19,32] These regions were also where the relative spacing of adjacent axial struts were arranged in close proximity (axial line D, Fig. 7). Interestingly, previous results indicate that greater amounts of dye became entrapped between adjacent computational struts when the spacing between stent struts was minimized.[3]

Regions of low wall shear stress were localized around stent struts. This observation is likely due to a combination of stagnation flow and boundary layer separation immediately upstream and downstream of the struts, respectively, as described by classic problems of a stationary block placed on a wall[36,38] and is consistent with the local accumulation of dye during flow visualization through Palmaz–Schatz stents.[2] Wall shear stress decreased with each subsequent axial strut due to the existence of the stent (Fig. 8) and suggests that stents designed with a minimum number of axial struts may limit the extent of adverse flow disturbances within the stented region of the vessel. The present results are supported by the observation that reducing the number of strut intersections limits the amount of subsequent intimal thickening and thrombus formation in rabbit iliac arteries.[27] The effect of angled stent struts in the present computational simulations also suggests that stent struts aligned in the axial direction of blood flow may be advantageous for limiting the flow disturbances within the stent. This conclusion is supported by a previous study comparing flow dye visualization wash-out times between the Palmaz–Schatz stent and a prototype stent with four longitudinal struts aligned parallel to the direction of blood flow.[2]

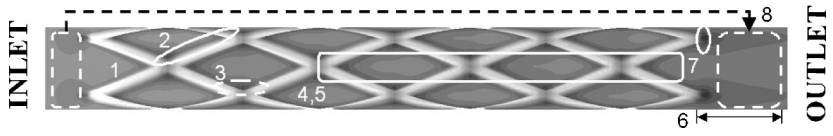

FIGURE 8. Summarized alterations in wall shear stress induced by the presence of a slotted-tube stent. (1) Angled struts act as converging and diverging nozzles to adjacent blood layers. (2) Low wall shear stress (τ_u) is localized around stent struts. (3) Lowest τ_u located in the corners of each strut. (4) Transient increases in τ_u proximal and distal to low τ_u regions. (5) τ_u decreases with each subsequent axial strut. (6) Reduced outlet τ_u lengthens as a function of inlet velocity. (7) Areas of low wall shear stress were noticed at transitions between the vessel and stent and were most pronounced where the strut orientation was orthogonal to the direction of blood flow. (8) Marked decrease in τ_u at the outlet of the stent as compared to the inlet.

The present results also indicate that regions of lower wall shear stress are more pronounced toward the outlet of the stent. Inlet velocity is a major determinant of the distance required for shear stress to approach a constant value at the stent outlet as regions of low wall shear stress were extended in this area for maximum inlet velocities, particularly during elevated flow conditions. This finding is consistent with those noted in previous studies where simulations of increased blood flow mimicking exercise were applied as boundary conditions to *in vitro* and computational studies.[2,3,25]

Several investigators have postulated that spatial wall shear stress gradients are associated with intimal thickening.[5,33,34] These wall shear stress gradients can cause conflicting forces on adjacent, normally confluent, cells, thus leading to increased cell division after wall shear stress perturbation.[5] When spatial wall shear stress gradients were calculated from the magnitude of differentiated wall shear stress distributions in the present investigation, the maximum value of the wall shear stress gradient corresponding to resting blood flow was 22 dyn/cm^2 per mm and occurred in the region near the proximal stent edge. Wall shear stress gradients of this magnitude have previously been associated with increased cellular proliferation and migration *in vitro*.[34]

The present results should be interpreted within the constraints of several potential limitations. The accuracy of CFD modeling of wall shear stress distributions is dependent upon the density of the computational mesh, and hence, the time to simulation convergence. All stented vessels contained a minimum of 369,834 nodes, and simulation results differed by 6% from the simulations using a coarser computational mesh. The majority of cells added to computational vessels were included in local areas of interest near stent struts and at the inlet and outlet of the stent. This level of error was deemed acceptable in a previous study examining mesh resolution in three-dimensional CFD models of the right coronary artery[22] and allowed for simulation convergence within 72 h. Additionally, the distributions of wall shear stress obtained in the present study are consistent with previous *in vivo* and computational studies.[12,14,17] Thus, it is unlikely that a greater number of circumferential and axial nodes would have resulted in different conclusions regarding the behavior of blood flow and patterns of wall shear stress in the stented computational models. The present investigation was conducted by applying steady-state boundary conditions to rigid straight computational arteries. These boundary conditions were employed to address the hypothesis of the investigation and elucidate areas of interest for future studies. Blood flow is undoubtedly pulsatile in the human body. Therefore, these simulation conditions represent a limitation of the present investigation as the results may differ for pulsatile flow. Nevertheless, three-dimensional CFD studies illustrating alterations in distributions of wall shear stress after stent implantation have not yet been reported. Previous studies indicate that a rigid wall assumption is valid within a stented vascular section,[1,9] but it may introduce error in the unstented portion of the vessel.[26] Blood was assumed to be a Newtonian fluid in the present investigation. It is possible that incorporation of non-Newtonian conditions, in which viscosity is a function of the shear rate, may result in distributions of shear stress slightly different than those presented here. Future studies will be necessary to examine the influence of non-Newtonian properties on distributions of wall shear stress in stented vascular segments. The native epicardial coronary arteries follow the curvature of the indwelling myocardium. Wentzel *et al.* reported that implantation of a Schneider wall stent caused straightening of an epicardial coronary artery *in vivo*.[41] Thus, the present results obtained using a computational assumption of straight stent geometry may represent a physiological approximation despite neglecting the curvature of the LAD coronary artery. Nonetheless, the assumption of straightness applied to stented simulations may underestimate alterations in wall shear stress due to centrifugal force and subsequent skewing of the velocity profile away from the midline of the vessel in regions immediately proximal and distal to the stent.

The present results were intended to illustrate changes in acute wall shear stress induced by stent implantation. It is highly likely that progressive endothelialization and smooth muscle cell proliferation around a chronically implanted stent would affect the distribution of wall shear stress *in vivo*. Nonetheless, initial smooth muscle cell migration and proliferation have been shown to reach a maximum at seven days after stent implantation.[6,19,29] Thus, an understanding of immediate and short-term contributions of wall shear stress alterations to this process remains an important goal of future research.

In summary, the present investigation describes alterations in wall shear stress caused by slotted-tube stent design in a three-dimensional CFD model of an epicardial coronary artery using *in vivo* data as boundary conditions. The present results were consistent with previous flow visualization findings and provide additional indirect support to the hypothesis that wall shear stress disturbances produced by stents may play a role in subsequent intimal hyperplasia and restenosis. The relative size of stent struts from one stent type to another does not vary greatly[13] and likely results in only small disparities in distributions of wall shear stress. However, restenosis varies distinctively with stent type suggesting that small wall shear stress disparities like those presented in the present investigation may contribute to the potential for restenosis following stent implantation. Mechanotransduction of shear forces responsible for

gene expression and protein synthesis may also be differentially influenced by these small differences in shear stress. Additional research will be required to define whether wall shear stress alterations produced by different stent geometries may preferentially contribute to intimal thickening and predispose the coronary artery to restenosis *in vivo*.

ACKNOWLEDGMENTS

The authors thank John P. Tessmer, John G. Krolikowski, David A. Schwabe (Research Scientists, Department of Anesthesiology, Medical College of Wisconsin, Milwaukee, WI), and David J. Powers (Computer Staff Engineer, Olin Engineering Center, Marquette University, Milwaukee, WI) for their technical assistance. This work was supported in part by Boston Scientific—Scimed and by the National Institute of Health: Grant Nos. HL-03690 and HL-63705 for one of the authors (J.R.K.), and Grant Nos. HL-54820 and GM-08377 for one of the authors (D.C.W.).

REFERENCES

[1] Back, M., G. Kopchok, M. Mueller, D. Cavaye, C. Donayre, and R. A. White. Changes in arterial wall compliance after endovascular stenting. *J. Vasc. Surg.* 19:905–911, 1994.

[2] Berry, J. L., J. J. E. Moore, V. S. Newman, and W. D. Routh. *In vitro* flow visualization in stented arterial segments. *J. Vasc. Invest.* 3:63–68, 1997.

[3] Berry, J. L., A. Santamarina, J. J. E. Moore, S. Roychowdhury, and W. D. Routh. Experimental and computational flow evaluation of coronary stents. *Ann. Biomed. Eng.* 28:386–398, 2000.

[4] Caramori, P. R., V. C. Lima, P. H. Seidelin, G. E. Newton, J. D. Parker, and A. G. Adelman. Long-term endothelial dysfunction after coronary artery stenting. *J. Am. Coll. Cardiol.* 34:1675–1679, 1999.

[5] DePaola, N., M. A. Gimbrone, P. F. Davies, and C. F. Dewey. Vascular endothelium responds to fluid shear stress gradients. *Arterioscler. Thromb.* 12:1254–1257, 1992.

[6] Edelman, E. R., and C. Rogers. Pathobiologic responses to stenting. *Am. J. Cardiol.* 81:4E–6E, 1998.

[7] Erbel, R., M. Haude, H. W. Hopp, D. Franzen, H. J. Rupprecht, B. Heublein, K. Fischer, P. de Jaegere, P. Serruys, W. Rutsch, and P. Probst. Coronary-artery stenting compared with balloon angioplasty for restenosis after initial balloon angioplasty. Restenosis Stent Study Group. *N. Engl. J. Med.* 339:1672–1678, 1998.

[8] Fischman, D. L., M. B. Leon, D. S. Baim, R. A. Schatz, M. P. Savage, I. Penn, K. Detre, L. Veltri, D. Ricci, and M. Nobuyoshi. A randomized comparison of coronary-stent placement and balloon angioplasty in the treatment of coronary artery disease. Stent Restenosis Study Investigators. *N. Engl. J. Med.* 331:496–501, 1994.

[9] Flueckiger, F., H. Sternthal, G. E. Klein, M. Aschauer, D. Szolar, and G. Kleinhappl. Strength, elasticity, and plasticity of expandable metal stents: *In vitro* studies with three types of stress. *J. Vasc. Interv Radiol.* 5:745–750, 1994.

[10] Fontaine, A. B., D. G. Spigos, G. Eaton, S. Das Passos, G. Christoforidis, H. Khabiri, and S. Jung. Stent-induced intimal hyperplasia: Are there fundamental differences between flexible and rigid stent designs? *J. Vasc. Interv Radiol.* 5:739–744, 1994.

[11] Hoffmann, R., G. S. Mintz, G. R. Dussaillant, J. J. Popma, A. D. Pichard, L. F. Satler, K. M. Kent, J. Griffin, and M. B. Leon. Patterns and mechanisms of in-stent restenosis. A serial intravascular ultrasound study. *Circulation* 94:1247–1254, 1996.

[12] Ilegbusi, O. J., Z. Hu, R. Nesto, S. Waxman, D. Cyganski, J. Kilian, P. H. Stone, and C. L. Feldman. Determination of blood flow and endothelial shear stress in human coronary artery *in vivo*. *J. Invasive Cardiol.* 11:667–674, 1999.

[13] Kastrati, A., J. Mehilli, J. Dirschinger, J. Pache, K. Ulm, H. Schuhlen, M. Seyfarth, C. Schmitt, R. Blasini, F. J. Neumann, and A. Schomig. Restenosis after coronary placement of various stent types. *Am. J. Cardiol.* 87:34–39, 2001.

[14] Kirpalani, A., H. Park, J. Butany, K. W. Johnston, and M. Ojha. Velocity and wall shear stress patterns in the human right coronary artery. *J. Biomech. Eng.* 121:370–375, 1999.

[15] Kohler, T. R., T. R. Kirkman, L. W. Kraiss, B. K. Zierler, and A. W. Clowes. Increased blood flow inhibits neointimal hyperplasia in endothelialized vascular grafts. *Circ. Res.* 69:1557–1565, 1991.

[16] Ku, D. N. Blood flow in arteries. *Annu. Rev. Fluid Mech.* 29:399–434, 1997.

[17] Ku, D. N., D. P. Giddens, C. K. Zarins, and S. Glagov. Pulsatile flow and atherosclerosis in the human carotid bifurcation. Positive correlation between plaque location and low oscillating shear stress. *Arteriosclerosis (Dallas)* 5:293–302, 1985.

[18] LaDisa, J. F., D. A. Hettrick, L. E. Olson, I. Guler, E. R. Gross, T. T. Kress, J. R. Kersten, D. C. Warltier, and P. S. Pagel. Coronary stent implantation alters coronary artery hemodynamics and wall shear stress during maximal vasodilation. *J. Appl. Physiol.* 93:1939–1946, 2002.

[19] Liu, S. Q., and J. Goldman. Role of blood shear stress in the regulation of vascular smooth muscle cell migration. *IEEE Trans. Biomed. Eng.* 48:474–483, 2001.

[20] Malek, A. M., S. L. Alper, and S. Izumo. Hemodynamic shear stress and its role in atherosclerosis. *J. Am. Med. Assoc.* 282:2035–2042, 1999.

[21] Moore, Jr., J. E., C. Xu, S. Glagov, C. K. Zarins, and D. N. Ku. Fluid wall shear stress measurements in a model of the human abdominal aorta: Oscillatory behavior and relationship to atherosclerosis. *Atherosclerosis* 110:225–240, 1994.

[22] Myers, J. G., J. A. Moore, M. Ojha, K. W. Johnston, and C. R. Ethier. Factors influencing blood flow patterns in the human right coronary artery. *Ann. Biomed. Eng.* 29:109–120, 2001.

[23] Newman, V. S., J. L. Berry, W. D. Routh, C. M. Ferrario, and R. H. Dean. Effects of vascular stent surface area and hemodynamics on intimal thickening. *J. Vasc. Interv. Radiol.* 7:387–393, 1996.

[24] Nichols, W. W., and M. F. O'Rourke. McDonald's Blood Flow in Arteries: Theoretical, Experimental and Clinical Principles, 4th ed. New York: Oxford University Press, 1998.

[25] Peacock, J., S. Hankins, T. Jones, and R. Lutz. Flow instabilities induced by coronary artery stents: Assessment with an *in vitro* pulse duplicator. *J. Biomech.* 28:17–26, 1995.

[26] Qiu, Y., and J. M. Tarbell. Numerical simulation of pulsatile flow in a compliant curved tube model of a coronary artery. *J. Biomech. Eng.* 122:77–85, 2000.

[27] Rogers, C., and E. R. Edelman. Endovascular stent design dictates experimental restenosis and thrombus. *Circulation* 91:2995–3001, 1995.

[28] Rogers, C., E. R. Edelman, and D. I. Simon. A mAb to the beta2-leukocyte integrin Mac-1 (CD11b/CD18) reduces intimal thickening after angioplasty or stent implantation in rabbits. *Proc. Natl. Acad. Sci. U.S.A.* 95:10134–10139, 1998.
[29] Rogers, C., F. G. P. Welt, M. J. Karnovsky, and E. R. Edelman. Monocyte recruitment and neointimal hyperplasia in rabbits. *Arterioscler., Thromb., Vasc. Biol.* 16:1312–1318, 1996.
[30] Sabbah, H. N., F. Khaja, E. T. Hawkins, J. F. Brymer, T. M. McFarland, J. van der Bel-Kahn, P. T. Doerger, and P. D. Stein. Relation of atherosclerosis to arterial wall shear in the left anterior descending coronary artery of man. *Am. Heart J.* 112:453–458, 1986.
[31] Schatz, R. A., J. C. Palmaz, F. O. Tio, F. Garcia, O. Garcia, and S. R. Reuter. Balloon-expandable intracoronary stents in the adult dog. *Circulation* 76:450–457, 1987.
[32] Serruys, P., P. De Jaegere, F. Kiemeneij, C. Macaya, W. Rutch, G. Heyndrickx, H. Emanuelsson, J. Marco, V. Legrand, P. Materne, J. Belardi, U. Sigwart, A. Colombo, J. J. Goy, v. d. H. P., D. J. Morel, and M.-A. Morel. A comparison of balloon-expandable-stent implantation with balloon angioplasty in patients with coronary heart disease. *N. Engl. J. Med.* 331:489–495, 1994.
[33] Tada, S., and J. M. Tarbell. Flow through internal elastic lamina affects shear stress on smooth muscle cells (3D simulations). *AJP-Heart Circ. Physiol.* 282:H576–H584, 2002.
[34] Tardy, Y., N. Resnick, T. Nagel, M. A. Gimbrone, and C. F. Dewey. Shear stress gradients remodel endothelial monolayers *in vitro* via a cell proliferation-migration-loss cycle. *Arterioscler., Thromb., Vasc. Biol.* 17:3102–3106, 1997.
[35] Tominaga, R., H. E. Kambic, H. Emoto, H. Harasaki, C. Sutton, and J. Hollman. Effects of design geometry of intravascular endoprostheses on stenosis rate in normal rabbits. *Am. Heart J.* 123:21–28, 1992.
[36] Tritton, D. J. Physical Fluid Dynamics. Oxford: Clarendon, 1988.
[37] van Beusekom, H. M., D. M. Whelan, S. H. Hofma, S. C. Krabbendam, V. W. van Hinsbergh, P. D. Verdouw, and W. J. van der Giessen. Long-term endothelial dysfunction is more pronounced after stenting than after balloon angioplasty in porcine coronary arteries. *J. Am. Coll. Cardiol.* 32:1109–1117, 1998.
[38] Van Dyke, M. An Album of Fluid Motion. Stanford: Parabolic, 1982.
[39] Vrints, C. J., M. J. Claeys, J. Bosmans, V. Conraads, and J. P. Snoeck. Effect of stenting on coronary flow velocity reserve: Comparison of coil and tubular stents. *Heart* 82:465–470, 1999.
[40] Wentzel, J. J., R. Krams, J. C. H. Schuurbiers, J. A. Oomen, J. Kloet, W. J. van der Giessen, P. W. Serruys, and C. J. Slager. Relationship between neointimal thickness and shear stress after wallstent implantation in human coronary arteries. *Circulation* 103:1740–1745, 2001.
[41] Wentzel, J. J., D. M. Whelan, W. J. van der Giessen, H. M. van Beusekom, I. Andhyiswara, P. W. Serruys, C. J. Slager, and R. Krams. Coronary stent implantation changes 3D vessel geometry and 3D shear stress distribution. *J. Biomech.* 33:1287–1295, 2000.
[42] Yoshitomi, Y., S. Kojima, M. Yano, T. Sugi, Y. Matsumoto, M. Saotome, K. Tanaka, M. Endo, and M. Kuramochi. Does stent design affect probability of restenosis? A randomized trial comparing Multilink stents with GFX stents. *Am. Heart J.* 142:445–451, 2001.